PNAS
www.pnas.org

Supplementary Information for
Symbiosis-inspired de novo synthesis of ultrahigh MOF growth mixed matrix membranes for sustainable carbon capture.

Shanshan He [a], Bin Zhu [a], Xu Jiang [b], Gang Han [c], Songwei Li [d], Cher Hon Lau [e], Yadong Wu [a], Yanqiu Zhang [a], Lu Shao*[a]

*Lu Shao
Email: shaolu@hit.edu.cn

This PDF file includes:

Supplementary text
Figures S1 to S15
Tables S1 to S7
SI References

Supplementary Information Text

Experimental Procedures.

Chemicals: The two monomers of 5,5',6,6'-tetrahydroxy-3,3,3',3'-tetramethyl-1,1'-spirobisindane (TTSBI, 97%, Alfa Aesar) and 2,3,5,6-tetrafluoroterephthalonitrile (TFTPN, 99%, Sigma-Aldrich) were purified before usage, according to well-established Peter M. Budd's method.(1) TTSBI was purified by dissolving in methanol and re-precipitating from dichloromethane. TFTPN was purified by sublimation. Anhydrous K_2CO_3 (99.0%, Sigma-Aldrich) was dried at 110 °C overnight before use. Zn $(NO_3)_2 \cdot 6H_2O$ and dimethylimidazole (Hmim) were purchased from Sigma-Aldrich. All solvents (Aladdin) containing dimethylformamide (DMF), cyclohexane, methanol (MeOH), and chloroform ($CHCl_3$) were used as received.

Synthesis of ZIF-8: 0.744 g Zn $(NO_3)_2 \cdot 6H_2O$ was dissolved in 20 g water and 12.3 g Hmim was dissolved in 80 g water. Zn $(NO_3)_2 \cdot 6H_2O$ aqueous solution was poured into Hmim aqueous solution, and then stirred for 1 h. The product was centrifuged and washed three times. The resultant ZIF-8 powder was dried and activated at 100 ℃ overnight.

The calculation of ZIF-8 loading in ZIF-8/PIM-1 MMMs: ZIF-8 loading in the MMMs was calculated according to the residual weight at 1000 °C after thermal treatment in the air (**Figure 1f**). The residual weight for pure PIM-1 and the ZIF-8/PIM-1 MMM was 0.22% and 24.14%, respectively, and the additional weight of the latter was derived from ZnO. According to the net weight

percentage of ZnO (i.e., 23.92%), the weight percentage of Zn could be obtained, and then the mass percent of ZIF-8 in MMMs was obtained by dividing the mass percentage of Zn in ZIF-8 (i.e., $C_8H_{10}N_4Zn$). Similarly, ZIF-7 and ZIF-67 loadings in PIM-1, and ZIF-8 loading in Matrimid could also be calculated via this method.

The traditional mixing method of ZIF-8/PIM-1 mixed matrix membranes: 0.1 g PIM-1 was dissolved in 5 mL $CHCl_3$, and 0.205 g ZIF-8 was dispersed in 5 mL $CHCl_3$, respectively. Then the ZIF-8 dispersion dropped into PIM-1 solution gradually for four times in 24 hours with continuous stirring. The mixture was ultrasonic for 0.5 h to remove bubbles before casting in the mold. The membrane was named as TM-67.2 wt%-ZIF-8/PIM-1.

Characterizations: Thermal gravimetric analysis (TGA) was carried out (r.t.~ 1000 °C, 10 °C min^{-1}, N_2 or air atmosphere) using a PerkinElmer TGA400 analyzer. X-ray diffraction (XRD) measurements were carried out on a Bruker D8 ADVANCE X-ray diffractometer at 40 kV and 40 mA Cu-Ka (λ=1.5418 A) with a scan speed of 5° min^{-1} and a scan range from 5° to 80°. Attenuated total reflectance Fourier transform infrared (ATR-FTIR) for the membrane surface was tested on a Spectrum One FT-IR spectrometer. X-ray photoelectron spectroscopy (XPS) analysis was determined using Shimadzu AXIS Ultra DLD with an Al-Kα X-ray source and the photoelectron take-off angle were 90° in regard to the specimen surface. The tensile strength of the membranes was measured using an electron tensile testing machine (CTM2050) with a drawing speed of 10 mm min^{-1}, the membrane samples were cut into 5 × 30 mm strips for the tensile test, each sample was tested three times. Gas adsorption/desorption was tested using 3H-2000PHD equipment (Beishide Instrument Technology Co., Ltd., China). All samples were measured after deaerating at 150 °C for 5 h. The gel-permeation chromatography (GPC) measurements presents the number-average molecular weight of PIM-1 is 21110 (Mn), the weight-average molecular weight is 77473 (Mw), and PDI (Mw/Mn) is 3.67.

Pure gas permeation test: Gas permeation measurements were conducted on a home-made constant-volume apparatus using the time-lag method. Gases were tested in the sequence of H_2, N_2, CH_4 and CO_2 under 35 °C and 3.5 atm. The gas permeability could be calculated by the following Equation S1:

$$P = \frac{273 \times 10^{10}}{760} \frac{Vl}{AT\left(p_2 \times \frac{76}{14.7}\right)} \frac{dp}{dt} \quad \text{(S1)}$$

Where dp/dt is the steady increase rate of downstream-pressure, V is the volume of the downstream chamber (cm^3), l is the membrane thickness (cm). A is the effective test area of the membrane (cm^2), T is the operating temperature (K) and p_2 is the upstream operating pressure (psi).

The gas permeation theory : The pure gas permeability (P) with the unit of Barrer (1 Barrer=10^{-10} cm^3(STP) cm/ (cm^2 s cm Hg) can be expressed by Fick's Law as the following Equation S2:

$$\mathrm{P} = \mathrm{D} \times \mathrm{S} \quad \text{(S2)}$$

Where D (cm^2/s) is the diffusion coefficient (diffusivity), S (cm^3 (STP) /cm^3 cm Hg) represents the sorption coefficient (solubility). The ideal selectivity of gas A over gas B ($\alpha_{a/b}$) is defined as the ratio of their permeabilities as Equation S3 shows:

$$\alpha_{\frac{A}{B}} = \frac{P_A}{P_B} = \left[\frac{D_A}{D_B}\right] \times \left[\frac{S_A}{S_B}\right] \quad \text{(S3)}$$

Using the diffusion time lag (θ) extrapolated from the plot of pressure with time (**Figure S2**) at steady state to the time axis, the diffusivity can be calculated by Equation S4:

$$D = \frac{l^2}{6\theta} \quad \text{(S4)}$$

Long-term gas permeation stability tests: Gas permeation stability was tested via pure gas permeation test. One membrane was cut into two halves for CO_2 and N_2 tests individually. CO_2 and N_2 tests were operated under continuous gas flow at 35 °C and 3.5 atm respectively. The testing operation lasted up to 240 h and the data were measured every 10 hours.

Plasticization tests: Plasticization behavior tests were performed via pure gas permeation test at 35 °C in a pressure range of 3.5 to 20 atm. The testing pressure was held at 3.5, 5, 7.5, 10, 15, and 20 atm for 0.5 h, respectively, after which the gas permeability was measured. Similarly, one

piece of the membrane was cut into two halves, one was used for CO_2 permeability test and the other was for N_2.

Gas permeability test at various temperatures: Gas permeabilities at different temperatures were conducted via pure gas permeation test. Gases were tested in the sequence of N_2, CH_4, and CO_2 at 3.5 atm, and the temperature was rapidly increased from 35 to 50 °C (i.e., 35, 40, 45, and 50 °C). The testing temperature was held at 35, 40, 45, and 50 °C for 2 h, respectively, after which the gas permeability was measured.

Binary gas test: The binary gas measurements were conducted on a Wicke−Kallenbach setup (Figure S3). Generally, the feed gas (20:80 mol% CO_2/N_2 mixture and 40:60 mol% CO_2/CH_4 mixture, respectively) were fed to the top surface of the membrane while Helium was used as the sweep gas on the permeate side. The test was run at 4.5 atm feed pressure and 35 °C with a feed gas flux of 50 mL/min and a sweep gas flux of 5 mL/min. The totally flux of the permeate gas were measured by a flow meter and the composition was analyzed by a gas chromatography (EchromA90). The separation factor Si/j of a binary mixture permeation is defined as the quotient of the molar ratios of the components (i, j) in the permeate, divided by the quotient of the molar ratio of the components (i, j) in the retentate as show in following Equation S5.

$$S_{i/j} = \frac{y_{i,Perm}/y_{j,Perm}}{y_{i,Ret}/y_{j,Ret}} \quad \text{(S5)}$$

Density functional theory (DFT) calculations for CO_2 adsorption energies in PIM-1 and ZIF-8: The projected augmented wave (PAW) potentials were chosen to describe the ionic cores and take valence electrons into account using a plane wave basis set with a kinetic energy cutoff of 450 eV. Partial occupancies of the Kohn−Sham orbitals were allowed using the Gaussian smearing method and a width of 0.05 eV. The electronic energy was considered self-consistent when the energy change was smaller than 10~5 eV. A geometry optimization was considered convergent when the energy change was smaller than 0.05 eV $Å^{-1}$. The vacuum spacing in a direction perpendicular to the plane of the structure is 15 Å. The Brillouin zone integration is performed using 1×1×1 Monkhorst-Pack k-point sampling for a structure. Finally, the adsorption energies (E_{ads}) were calculated as $E_{ads}= E_{ad/sub}-E_{ad}-E_{sub}$, where $E_{ad/sub}$, E_{ad}, and E_{sub} are the total energies of the optimized adsorbate/substrate system, the adsorbate in the structure, and the clean substrate, respectively.

The computational methodology of simulations for the interface of ZIF-8 and PIM-1: The density functional theory calculations and force field-based molecular dynamics simulations were used to confirm the good interface via simulating the interaction between the NH terminal functions of the organic linker at the ZIF-8 surface with -CN, -OH, and $-CH_3$ groups of PIM-1, respectively. The simulation calculation was conducted on four structures with an integration time-step of 2 fs. Periodic boundary conditions were applied in the x- and y-dimensions. The box size of the samples was $4.4 \times 4.4 \times 3.2$ nm^3. First, the conjugate gradient algorithm and energy minimization were performed to obtain a stable structure. Condensed-phased optimized molecular potential for atomistic simulation studies force field was also used to optimize these structures (ZIF-8 and PIM-1) in the Materials studio with forcite Module. Each sample was then equilibrated under the NPT ensemble at a constant temperature of 300 K to achieve an equilibrium state with zero pressure for 200 ns. The equilibration molecular systems of the pure separation membrane could be obtained after geometrically optimizing structure. Furthermore, a potential cutoff radius of 2.25 nm is applied in the calculation of the non-bonded interaction. And the PPPM has been used to describe the electrostatic. The Andersen feedback thermostat and Berendsen barostat algorithm are applied in the system with temperature and pressure conversion. Finally, the properties of our structures are obtained in the last 5 ns. The radial distribution functions (RDFs), g(r), give the probability of molecules occurring at the distance (r).

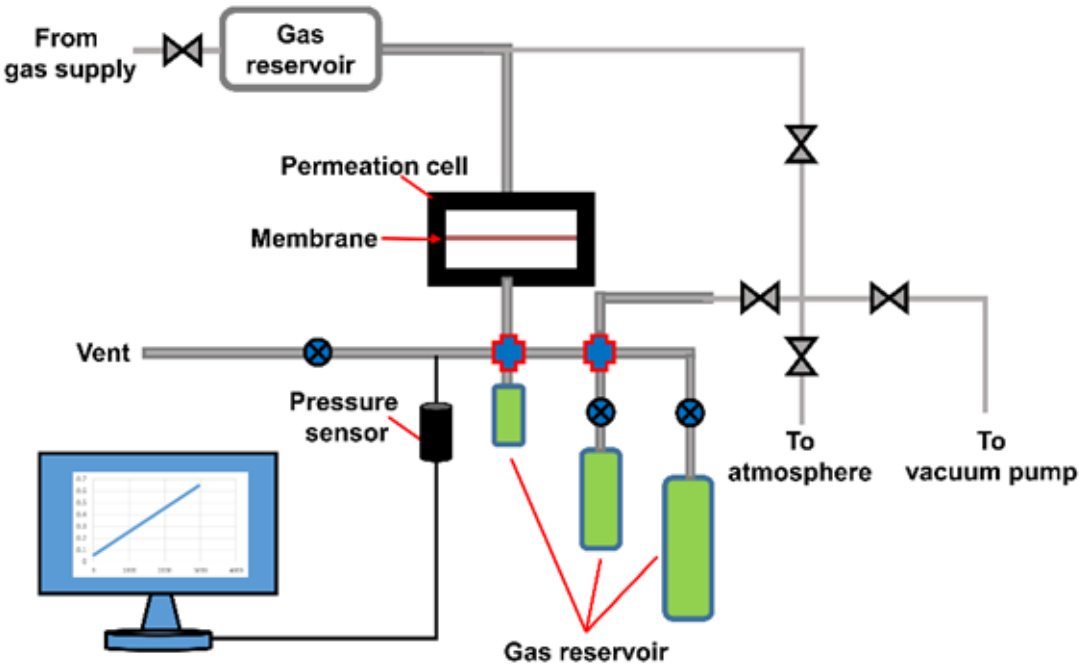

Figure S1 The illustration of the home-made apparatus for gas permeation test.

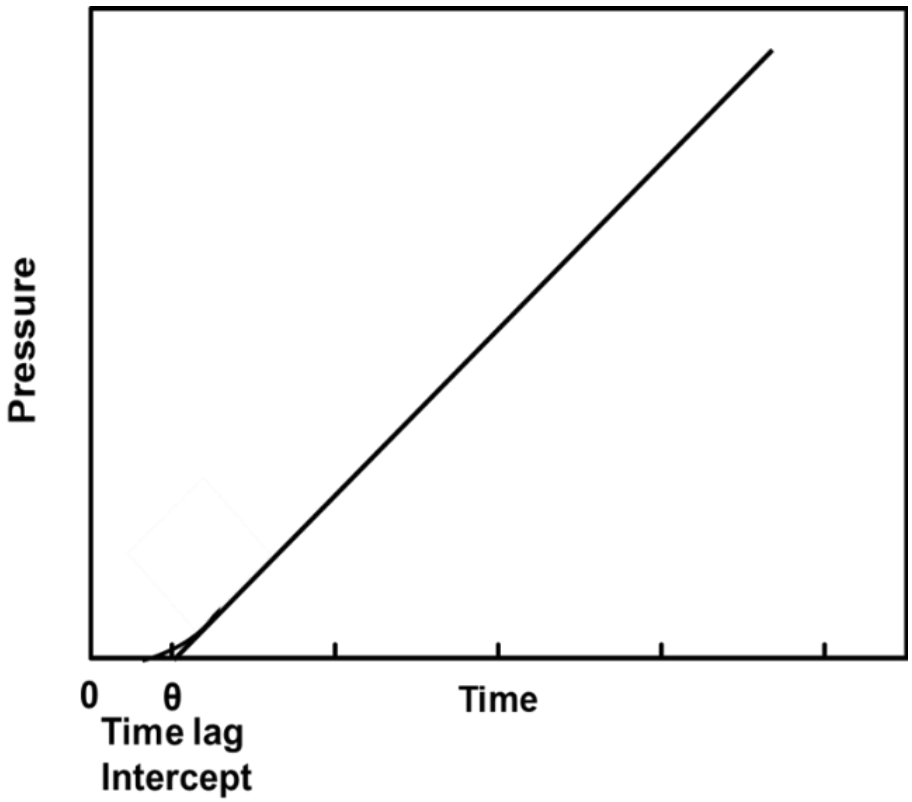

Figure S2 Time-lag derived from the gas permeation curves.

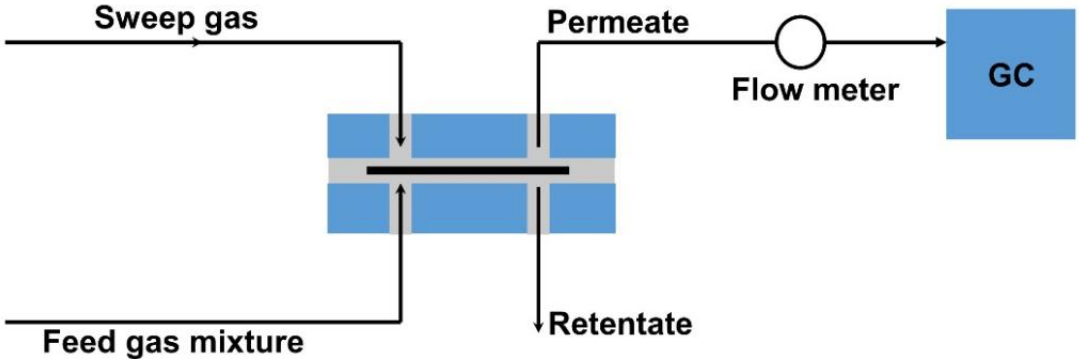

Figure S3 The binary gas permeation measurement set up.

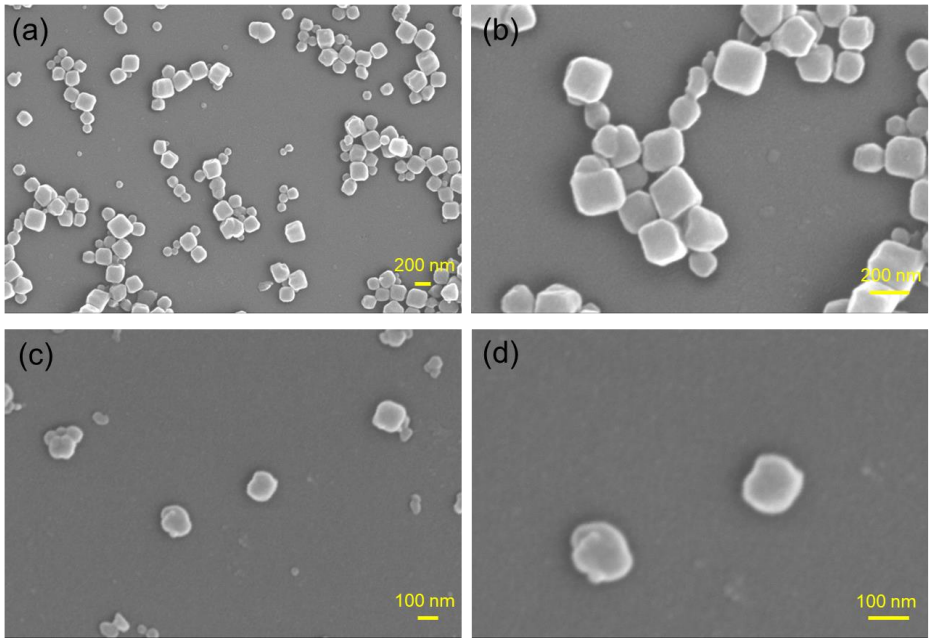

Figure S4 (a, b) ZIF-8 prepared via aqueous solution, and (c, d) ZIF-8 prepared via water/$CHCl_3$ mixture in this work.

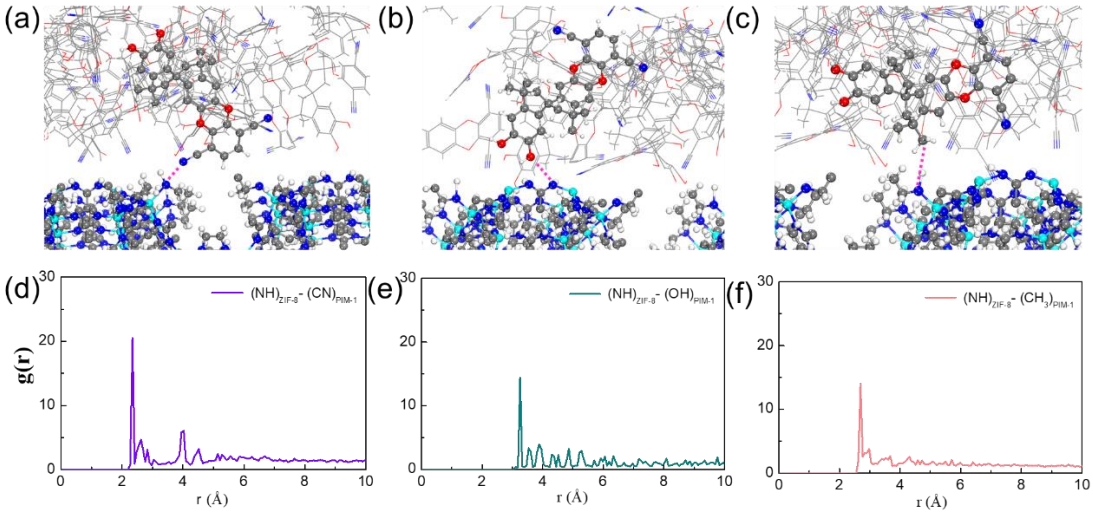

Figure S5 Illustration of (a) $(NH)_{ZIF\text{-}8}\cdots(CN)_{PIM\text{-}1}$ interaction, (b) $(NH)_{ZIF\text{-}8}\cdots(OH)_{PIM\text{-}1}$ interaction, and (c) $(NH)_{ZIF\text{-}8}\cdots(CH_3)_{PIM\text{-}1}$ interaction. The following color code is used for the atoms: Zn, light blue; N, dark blue; C, gray; H, white; O, red. Radial distribution functions for the pairs (d) $(NH)_{ZIF\text{-}8}\cdots(CN)_{PIM\text{-}1}$, (e) $(NH)_{ZIF\text{-}8}\cdots(OH)_{PIM\text{-}1}$, and (f) $(NH)_{ZIF\text{-}8}\cdots(CH_3)_{PIM\text{-}1}$ calculated for PIM-1/ ZIF-8 surface.

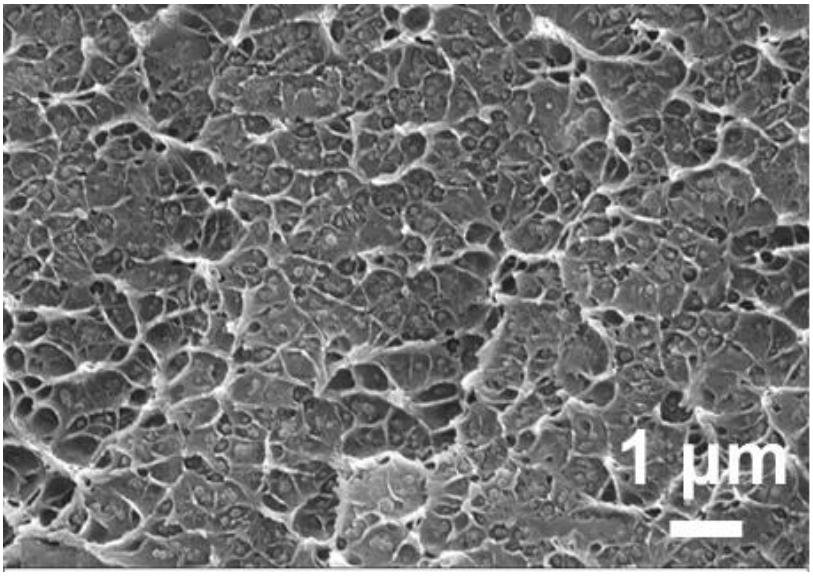

Figure S6 SEM cross-sectional images of 0.1-ZIF-8/PIM-1.

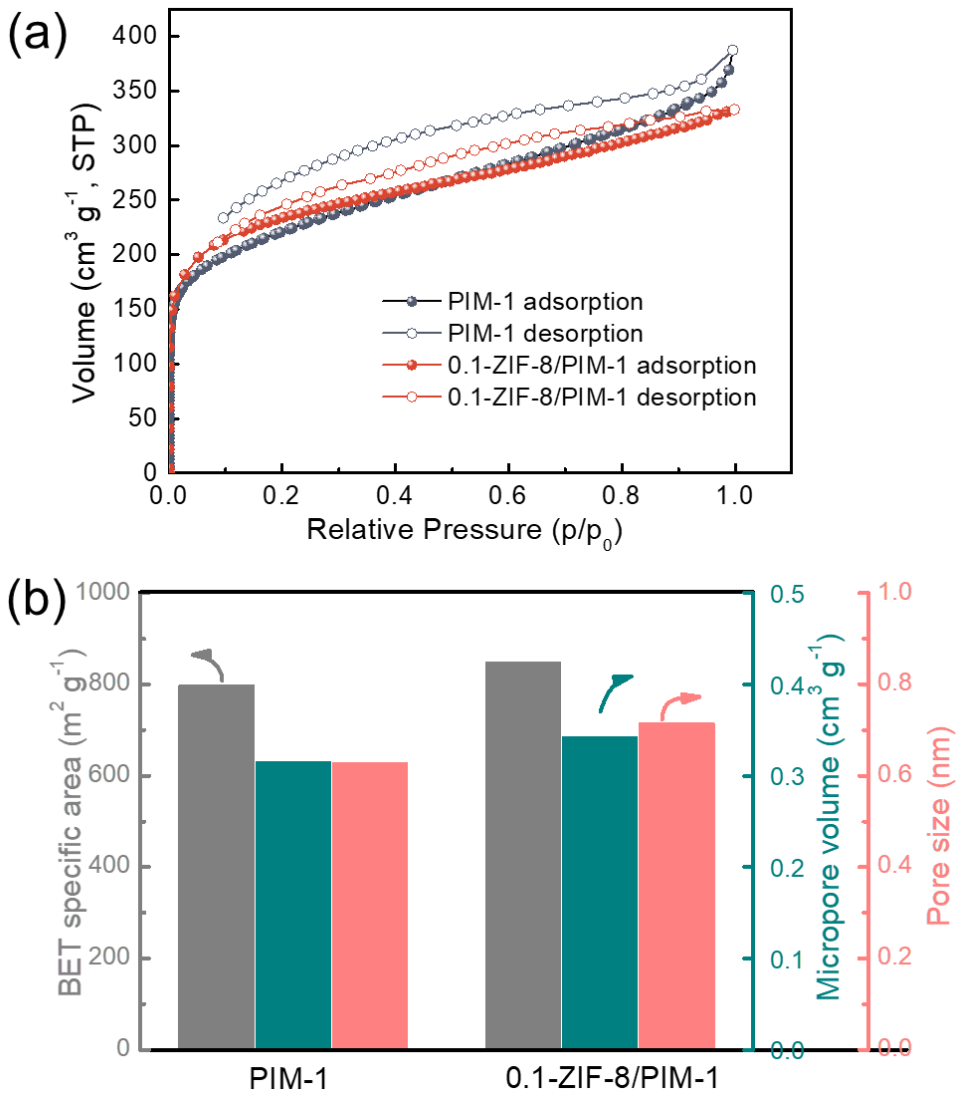

Figure S7 (a) N_2 adsorption/desorption isotherm (77 K) and (b) BET specific area, micropore volume and pore size of PIM-1 and 0.1-ZIF-8/PIM-1 membranes.

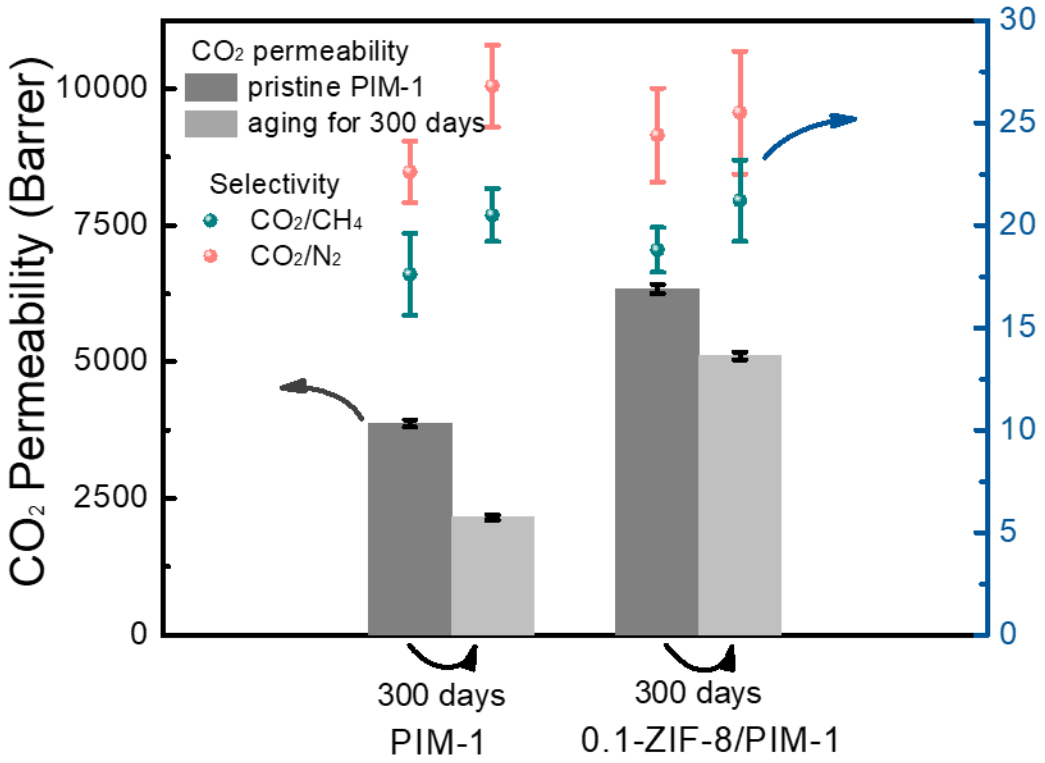

Figure S8 CO_2 separation performance of PIM-1 and 0.1-ZIF-8/PIM-1 membranes after natural aging for 300 days.

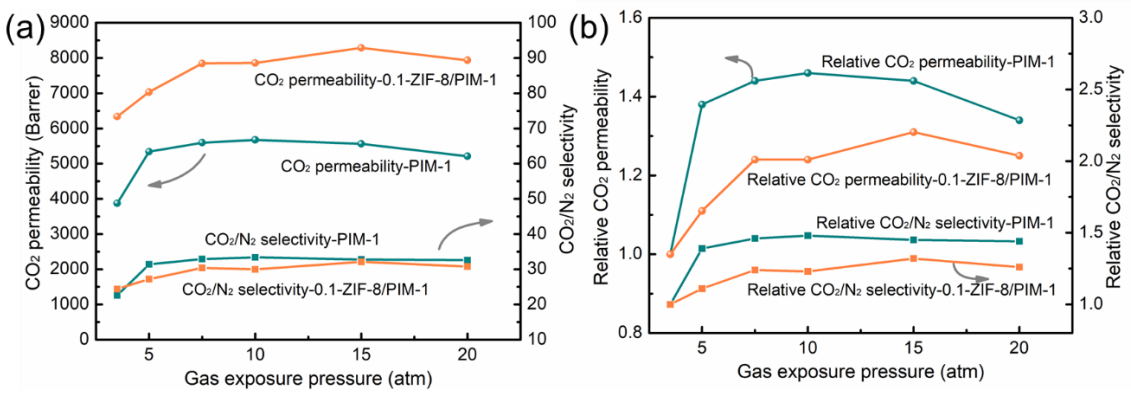

Figure S9 CO_2 permeability and CO_2/N_2 selectivity of PIM-1 and 0.1-ZIF-8/PIM-1 membranes at different gas exposure pressure.

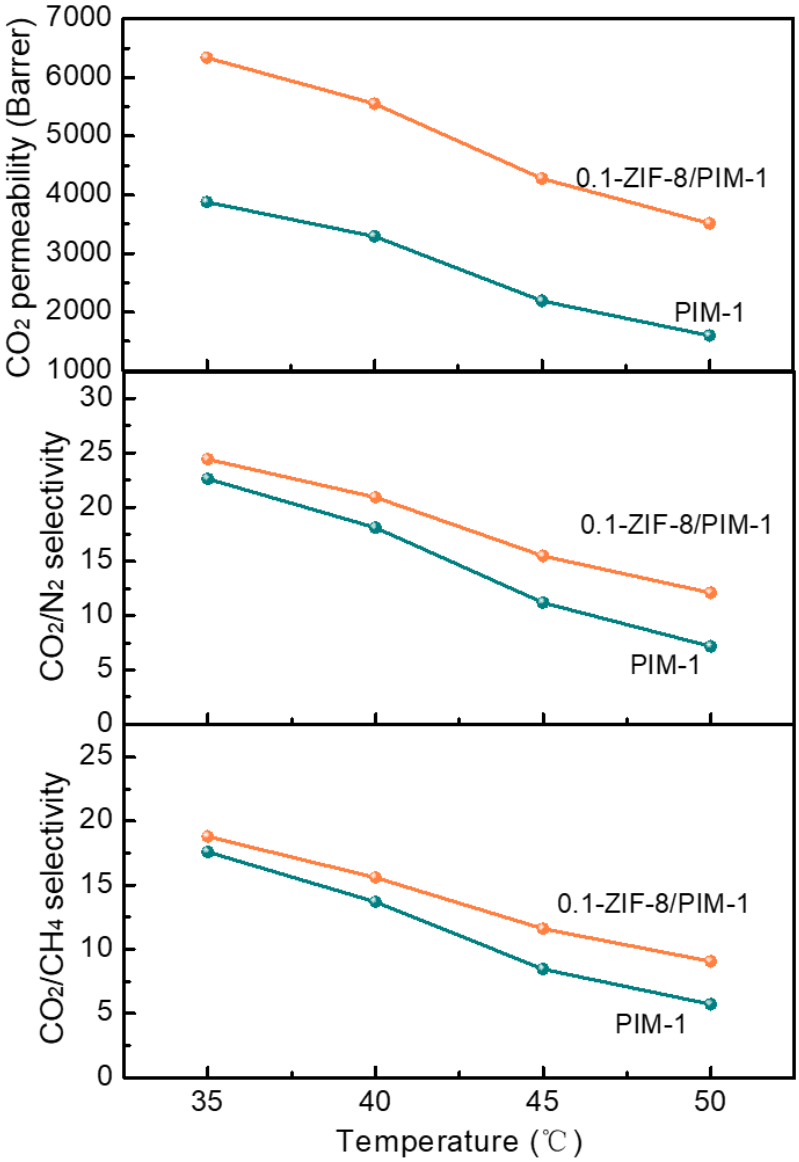

Figure S10 CO_2 separation performance at different temperatures (i.e., 35–50 °C)

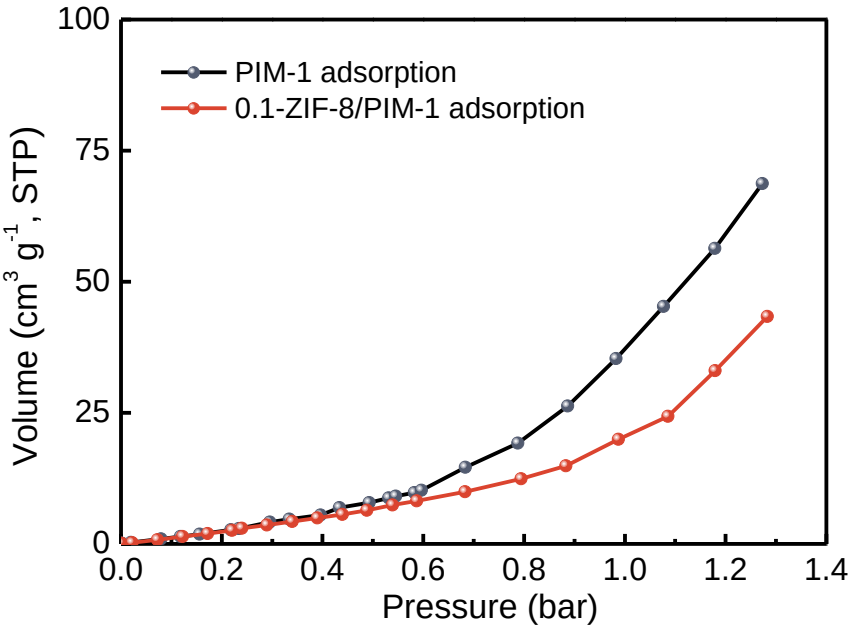

Figure S11 CH_4 adsorption isotherms of the 0.1-ZIF-8/PIM-1 and PIM-1 benchmark at 308 K.

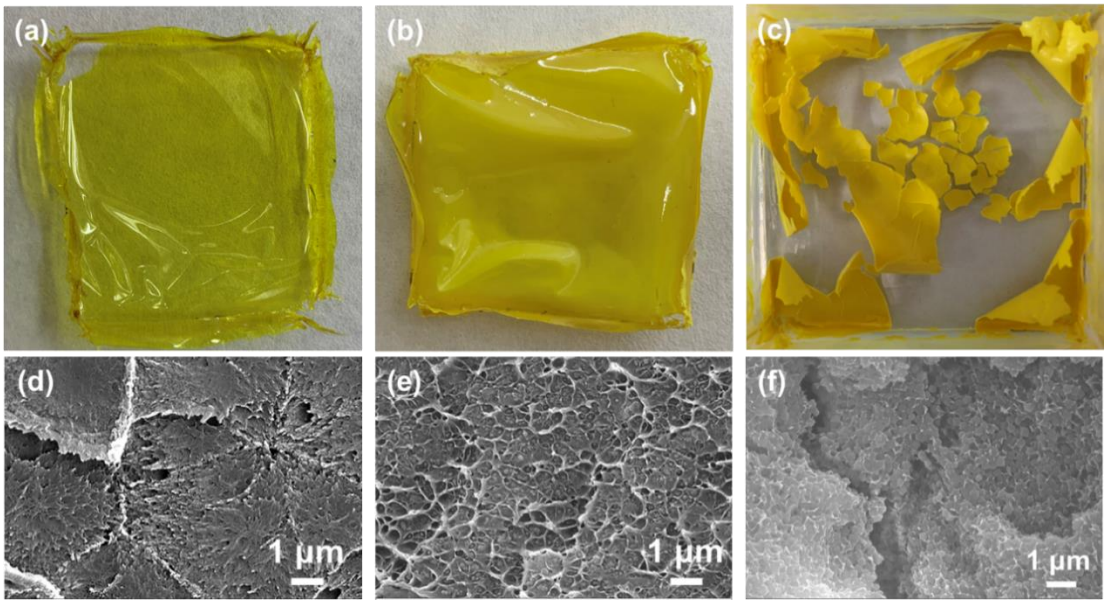

Figure S12 Digital photo (a~c) and cross-sectional SEM images (d~f) of pure PIM-1, 0.1-ZIF-8/PIM-1, and TM-67.2 wt.%-ZIF-8/PIM-1 membrane, respectively.

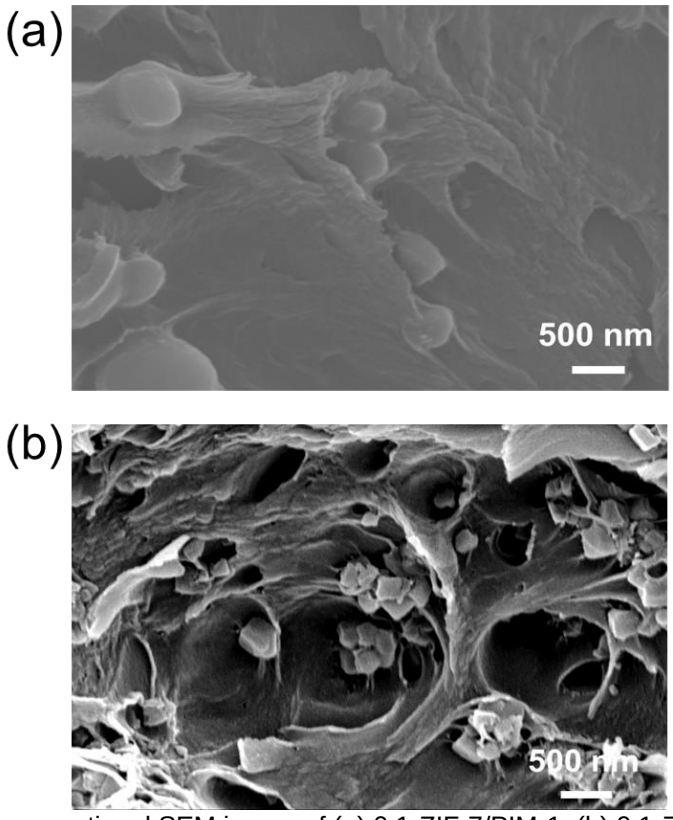

Figure S13 Cross-sectional SEM image of (a) 0.1-ZIF-7/PIM-1, (b) 0.1-ZIF-67/PIM-1.

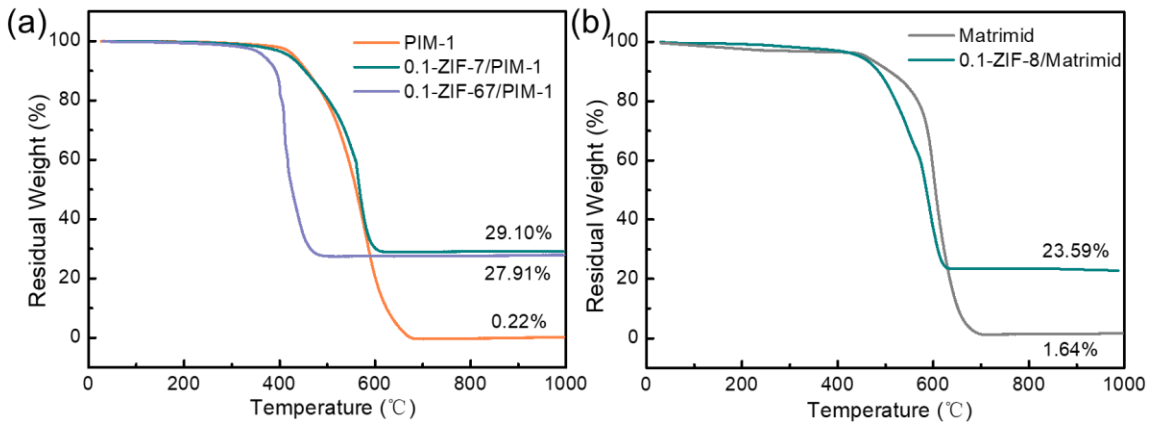

Figure S14 TGA curves of (a) pure PIM-1, 0.1-ZIF-7/PIM-1 and 0.1-ZIF-67/PIM-1, (b) Matrimid and 0.1-ZIF-8/Matrimid at air atmosphere.

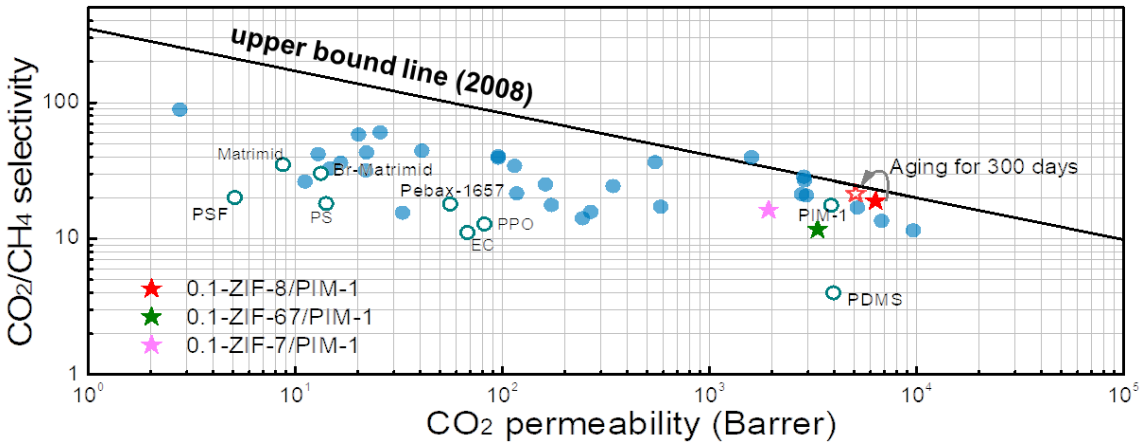

Figure S15 Selectivity versus permeability for CO_2/CH_4, where gas separation performance of the MMMs prepared in this work (pentacles), primary common polymeric membranes (hollow circles) and various MOF-based MMMs from literatures (solid circles) plotted against the Robeson plot of 2008(2). A fully detailed comparison of the data in this plot could be found in the **Table S6**.

Table S1. Gas permeability and selectivity of ZIF-8/PIM-1 MMMs at 3.5 bar and 35 °C.

Membranes	Permeability (Barrer)				Selectivity			
	CO_2	H_2	N_2	CH_4	CO_2/N_2	CO_2/CH_4	H_2/N_2	H_2/CH_4
PIM-1	3874±67	2884±59	171.4±20	220.4±32	22.6±1.5	17.6±2.0	16.8±1.5	13.1±1.2
0.05-ZIF-8/PIM-1	4027±98	2872±73	162.6±18	255.3±34	24.8±2.1	15.8±1.7	17.7±2.9	11.2±2.3
0.1-ZIF-8/PIM-1	6338±86	2860±69	259.5±25	336.4±27	24.4±2.3	18.8±1.1	11.0±3.1	8.50±1.2
0.15-ZIF-8/PIM-1	7629±77	4669±74	583.5±32	841.4±38	13.1±0.7	9.07±0.7	8.00±0.8	5.55±0.2
0.2-ZIF-8/PIM-1	9321±102	6759±83	783.0±45	1039±42	11.9±0.8	8.97±0.9	8.63±0.7	6.51±0.3

Table S2. The diffusivity and solubility and corresponding selectivity of membranes.

	CO_2		N_2		CH_4		CO_2/N_2		CO_2/CH_4	
	D [a]	S [b]	D	S	D	S	α(D)	α(S)	α(D)	α(S)
PIM-1	3.592	10.78	0.4006	4.279	0.3739	5.896	8.97	2.52	9.61	1.83
0.05-ZIF-8/PIM-1	0.8162	49.34	0.3036	5.356	0.3937	6.486	2.69	9.21	2.07	7.61
0.1-ZIF-8/PIM-1	1.704	37.19	1.898	1.367	0.7713	4.361	0.898	27.2	2.21	8.53
0.15-ZIF-8/PIM-1	10.40	7.336	13.7	0.4259	5.127	1.641	0.759	17.2	2.03	4.47
0.2-ZIF-8/PIM-1	25.40	3.668	39.17	0.1999	10.80	0.9614	0.648	18.35	2.35	3.82

[a] D $\times 10^{-7}$ cm^2/s; [b] S $\times 10^{-1}$ cm^3/cm^3 cm Hg

Table S3 Comparison of the CO_2 permeability and CO_2/gases selectivity of 0.1-ZIF-8/PIM-1 MMM in this work with other reported MOF/PIM-1 MMMs.

MOF	Loading (wt%)	Measurement conditions	CO_2 enhancement (%)	CO_2/N_2 selectivity enhancement (%)	CO_2/CH_4 selectivity enhancement (%)	Ref.
ZIF-8	67.2	35 °C, 3.5 bar	64	8.0	6.8	This work
ZIF-67	20	30 °C, 2 bar	15	20	34	(3)
Nano-sized ZIF-67 (ZIF-S)	15	30 °C, 2 bar	-38	--	69	(4)
NH_2-ZIF-7	20	30 °C, 2 bar	-35	--	65	(5)
UiO-66-NH2@IL	10	20 °C, 1 bar	18	5.0	51	(6)
Azo-UiO-66	10	20 psi, 298 K	79	0	--	(7)
UiO-66-NH_2	10	25 °C, 4 bar	-6.0	71	95	(8)
UiO-66-NH_2	7	35 °C, 1 bar	32	7.1	1.2	(9)
ZIF-8	--	25 °C, 1 bar	-78	32	48	(10)

Table S4 Mixed-gas separation performance of PIM-1 and 0.1-ZIF-8/PIM-1

Membranes	CO_2 Permeability (Barrer)				Selectivity	
	CO_2 [a]	N_2 [a]	CO_2 [b]	CH_4 [b]	20:80 mol% CO_2/N_2	40:60 mol% CO_2/CH_4
PIM-1	3756±10.3	174.7±5.0	3663±9.6	234.8±6.7	21.5±1.3	15.6±0.8
0.1-ZIF-8/PIM-1	6242±19.4	266.7±10.5	6186±20.5	374.9±8.9	23.4±1.2	16.5±1.3

[a] Gas permeability in 20:80 mol% CO_2/N_2 mixed gas; [b] Gas permeability in 40:60 mol% CO_2/CH_4 mixed gas

Table S5 The CO_2 and CH_4 adsorption capacity of the 0.1-ZIF-8/PIM-1 and PIM-1 benchmark at 308 K and 1.3 bar.

	C_{CO2} ($cm^3\ g^{-1}$(STP))	C_{CH4} ($cm^3\ g^{-1}$(STP))	$\alpha(S_{CO2/CH4})$
PIM-1	108.7	68.69	1.58
0.1-ZIF-8/PIM-1	124.1	43.38	2.86

Table S6 Comparison of the CO_2 permeability and CO_2/gases selectivity of MMMs in this work with other reported MMMs.

Polymer	MOF	Loading (wt.%)	Measurement conditions	CO_2 Permeability (Barrer)	CO_2/N_2 Selectivity	CO_2/CH_4 Selectivity	Ref.
PIM-1	ZIF-67	20	30 °C, 2 bar	5206±210	24.2±1.9	16.8±1.4	(3)
PIM-1	Nano-sized ZIF-67 (ZIF-S)	15	30 °C, 2 bar	2805±203	~24	21.09	(4)
PIM-1	NH_2-ZIF-7	20	30 °C, 2 bar	2953±266	--	20.6±0.6	(5)
PIM-1	CuBDC-ns	10	25 °C, 1 bar	268.62	--	15.6	(11)
PIM-1	UiO-66-NH_2	10	25 °C, 4 bar	2869±155	27.5±1.9	28.3±1.9	(8)
PIM-1	ZIF-8	32.4	20 °C, 1 bar	6820	17.9	13.4±1.3	(12)
PIM-1	ZIF-8 (120 nm)	5	4.0 bar	9700	--	11.4	(13)
Matrimid	dopamine decorated ZIF-8	40	35 °C, 3.5 atm	22	25.3	31.4	(14)
Matrimid	ZIF-8	20	22 °C, 4 bar	12.96	21.2	41.5	(15)
Matrimid	CuBDC (nanosheet)	8.2	25 °C,7.5 bar, CO_2/CH_4 equimolar	2.78	--	88.2	(16)
Matrimid	Ni_2(dodbc)	23	35 °C, 10 bar, equimolar CO_2/CH_4	14.7	--	32.5	(17)
Matrimid	ZIF-8	20	22 °C, 4 bar	16.63	19.0	35.8	(14)
Matrimid	GO-ZIF-8	20	30 °C, 1 bar	238	65	--	(18)
Matrimid	PEG 200& ZIF-8	30	8 bar, equimolar CO_2/CH_4	33.1	--	15.4	(19)
PEG/PPG-PDMS	UiO-66-NB	3	30 °C, 1 atm	585	--	~17	(20)
Pebax	ZIF-8	2	35 °C, 11 bar,	117.9	59	21.4	(21)
Pebax	ZIF-67	5	35 °C, 11 bar,	162	--	24.9	(21)
Pebax	ZIF-7	34	20 °C, 3.75 bar (CO_2), 7.5 bar (CH_4)	41	105	44	(22)
Pebax	ZIF-7-NH_2	31	35 °C, 4 bar	96	--	40	(23)
Pebax	ZIF-8-90	5	20 °C, 1 atm	99.7	59.6	--	(24)
PSF	PSF-embedded NH_2-UiO-66	10	2 atm	11.2	--	26.1	(25)
PSF	ZIF-11	24	25 °C, 3 bar	22.14	--	42.7	(26)
PEO	ZIF-8	67.7	35 °C, 5 bar	1083.7	38.5	--	(27)

PPO	Cu-BTC	40	30 ℃	115	26	34	(28)
PVC-g-POEM	ZIF-8	28.7	35 °C, 1 bar	244.9	39.3	14.0	(29)
cellulose nanofibers	ZIF-8	70	25 °C, 3 bar	550	45.5	36.2	(30)
Pebax-1657	PEI-ZIF-8	5	25 °C, CO_2/N_2 (50/50 vol%)	13	49	--	(31)
Pebax-1657	GO/core shell ZIF-8@ZIF-67	5	35 °C, 4 bar	173.2	61.9	17.5	(32)
Pebax-1657	ZIF-7-NH_2	31	35 °C, 4 bar, CO_2/CH_4 (50/50 vol%)	96	--	39	(23)
Pebax-1657	MWCNTs@ZIF-8	8	35 °C, 5 bar	186.3	61.3	--	(33)
Pebax-1657	NH_2-ZIF-8	6	25 °C, 1 bar	163.8	62	--	(34)
Pebax-1657	ZIF-8@GO	20	25 °C, 3 bar	136.2	77.9	--	(35)
Pebax-1074	EDD-ZIF-8	30	25 °C, 15 bar	344	--	24.2	(36)
6FDA-DAM:DABA (3:1)	GO and ZIF-8 (particle size of <40 nm)	1 wt%GO, 5 wt% ZIF-8	25 °C, 2 bar, CO_2/CH_4 (50/50 vol%)	1607.2	--	39.4	(37)
6FDA-BI	ZIF-8	20	35 °C, 4 bar	20.3	25.9	57.9	(38)
PEBA	MOF-808	7.5	20 °C, 1 bar CO_2/N_2 (50/50 vol%)	~22	66	--	(39)
PIM-1/6FDA-DAM 10/90 (w/w)	ZIF-8	10	50/50 CO_2/CH_4, 10/90 CO_2/N_2	2802/2891	18.1	26.6	(40)
PES	etched ZIF-8	--	--	15.7	6.5	--	(41)
PEI	(UiO-66-PEI@[bmim][Tf2N]	15	35 °C, 1 bar, CO_2/CH_4 (50/50 vol%)	25.86	--	59.99	(42)
Poly(styrene-co-butadiene)	Thermal-annealed ZIF-8	20	--	39.74	22	--	(43)
SBS-g-POEM	ZIF-8	15	35 °C, 1 bar	522.3	20.8	--	(44)
Pebax-1657	--	--	35 °C, 4 bar	56	--	18	(23)
PSF	--	--	2 atm	5.1	--	20	(25)
Matrimid	--	--	35 °C, 3.5 atm	8.7	29	35	(14)
Brominated Matrimid® 5218	--	--	35 °C, 10 atm	13.3	24.2	30.2	(45)
PDMS	--	--	35 °C, 4 bar	3970	6.7	4	(46)

Polystyrene (PS)	--	--	23 °C, 4.4 atm	14.1	28.8	18.1	(47)
PPO	--	--	35 °C, 1 atm	82	24.5	12.8	(48)
Ethyl cellulose (EC)	--	--	25 °C, 2 bar	67.7	21.3	11.1	(49)
PIM-1	--	--	35 °C, 3.5 atm	3874	22.6	17.6	This work

Table S7 Gas permeability and selectivity of Matrimid and ZIF-8/matrimid MMMs at 3.5 bar and 35 ^{o}C.

Membranes	Permeability (Barrer)				Selectivity			
	CO_2	H_2	N_2	CH_4	CO_2/N_2	CO_2/CH_4	H_2/N_2	H_2/CH_4
Matrimid	8.7	26	0.3	0.25	34.8	29	86.7	104
0.1-ZIF-8/Matrimid	37.5	100.2	1.448	1.263	29.7	25.9	69.2	79.3

SI References

1. Budd PM*, et al.* (2004) Polymers of intrinsic microporosity (PIMs): robust, solution-processable, organic nanoporous materials. *Chem Commun (Camb)* (2):230-231.
2. Robeson LM (2008) The upper bound revisited. *Journal of Membrane Science* 320(1-2):390-400.
3. Wu X*, et al.* (2018) Nanoporous ZIF-67 embedded polymers of intrinsic microporosity membranes with enhanced gas separation performance. *Journal of Membrane Science* 548:309-318.
4. Ye C*, et al.* (2020) Incorporating nano-sized ZIF-67 to enhance selectivity of polymers of intrinsic microporosity membranes for biogas upgrading. *Chemical Engineering Science* 216:115497.
5. Wang Y*, et al.* (2020) Amino-functionalized ZIF-7 embedded polymers of intrinsic microporosity membrane with enhanced selectivity for biogas upgrading. *Journal of Membrane Science* 602:117970.
6. Lu J*, et al.* (2021) Preparation of Amino-Functional UiO-66/PIMs Mixed Matrix Membranes with [bmim][Tf2N] as Regulator for Enhanced Gas Separation. *Membranes* 11(1).
7. Prasetya N & Ladewig BP (2019) An insight into the effect of azobenzene functionalities studied in UiO-66 frameworks for low energy CO_2 capture and CO_2/N_2 membrane separation. *Journal of Materials Chemistry A* 7(25):15164-15172.
8. Ghalei B*, et al.* (2017) Enhanced selectivity in mixed matrix membranes for CO_2 capture through efficient dispersion of amine-functionalized MOF nanoparticles. *Nature Energy* 2(7):17086.
9. Wang Z, Ren H, Zhang S, Zhang F, & Jin J (2017) Polymers of intrinsic microporosity/metal–organic framework hybrid membranes with improved interfacial interaction for high-performance CO_2 separation. *J. Mater. Chem. A* 5(22):10968-10977.
10. Fuoco A*, et al.* (2017) Synthesis and Transport Properties of Novel MOF/PIM-1/MOF Sandwich Membranes for Gas Separation. *Membranes* 7(1):7.
11. Cheng Y*, et al.* (2017) Ultrathin mixed matrix membranes containing two-dimensional metal-organic framework nanosheets for efficient CO_2 /CH_4 separation. *Journal of Membrane Science* 539:213-223.
12. Bushell AF*, et al.* (2013) Gas permeation parameters of mixed matrix membranes based on the polymer of intrinsic microporosity PIM-1 and the zeolitic imidazolate framework ZIF-8. *Journal of Membrane Science* 427:48-62.
13. Yahia M*, et al.* (2021) Effect of incorporating different ZIF-8 crystal sizes in the polymer of intrinsic microporosity, PIM-1, for CO_2/CH_4 separation. *Microporous and Mesoporous Materials* 312:110761.
14. Jiang X*, et al.* (2021) Aqueous One-Step Modulation for Synthesizing Monodispersed ZIF-8 Nanocrystals for Mixed-Matrix Membrane. *ACS applied materials & interfaces* 13(9):11296-11305.
15. Song Q*, et al.* (2012) Zeolitic imidazolate framework (ZIF-8) based polymer nanocomposite membranes for gas separation. *Energy & Environmental Science* 5(8):8359.
16. Rodenas T*, et al.* (2015) Metal-organic framework nanosheets in polymer composite materials for gas separation. *Nature materials* 14(1):48-55.
17. Bachman JE & Long JR (2016) Plasticization-resistant Ni2(dobdc)/polyimide composite membranes for the removal of CO2 from natural gas. *Energy & Environmental Science* 9(6):2031-2036.
18. Huang D*, et al.* (2018) Synergistic effects of zeolite imidazole framework@graphene oxide composites in humidified mixed matrix membranes on CO_2 separation. *RSC Advances* 8(11):6099-6109.
19. Castro-Muñoz R, Fíla V, Martin-Gil V, & Muller C (2019) Enhanced CO_2 permeability in Matrimid® 5218 mixed matrix membranes for separating binary CO_2/CH_4 mixtures. *Separation and Purification Technology* 210:553-562.
20. Hossain I, Husna A, Chaemchuen S, Verpoort F, & Kim T-H (2020) Cross-linked Mixed-Matrix Membranes using functionalized UiO-66-NH_2 into PEG/PPG–PDMS-Based rubbery

polymer for efficient CO_2 separation. *ACS Applied Materials & Interfaces* 12(52):57916-57931.

21. Meshkat S, Kaliaguine S, & Rodrigue D (2020) Comparison between ZIF-67 and ZIF-8 in Pebax® MH-1657 mixed matrix membranes for CO_2 separation. *Separation and Purification Technology* 235:116150.
22. Li T, Pan Y, Peinemann K-V, & Lai Z (2013) Carbon dioxide selective mixed matrix composite membrane containing ZIF-7 nano-fillers. *Journal of Membrane Science* 425-426:235-242.
23. Qian J*, et al.* (2020) Improved CO_2/CH_4 separation performance of mixed-matrix membrane by adding ZIF-7-NH_2 nanocrystals. *Journal of Applied Polymer Science* 138(20):50424.
24. Zheng W*, et al.* (2019) ZIF-8 nanoparticles with tunable size for enhanced CO_2 capture of Pebax based MMMs. *Separation and Purification Technology* 214:111-119.
25. Wu W, Su P, & Li W (2020) Mixed matrix membranes containing polymer‐embedded metal‐organic framework microspheres. *AIChE Journal* 66(11).
26. Guo A*, et al.* (2020) Molecular sieving mixed matrix membranes embodying nano-fillers with extremely narrow pore-openings. *Journal of Membrane Science* 601:117880.
27. Ma L, Svec F, Lv Y, & Tan T (2019) In situ bottom–up growth of metal–organic frameworks in a crosslinked poly(ethylene oxide) layer with ultrahigh loading and superior uniform distribution. *Journal of Materials Chemistry A* 7(35):20293-20301.
28. Ge L, Zhou W, Rudolph V, & Zhu Z (2013) Mixed matrix membranes incorporated with size-reduced Cu-BTC for improved gas separation. *Journal of Materials Chemistry A* 1(21):6350.
29. Lee CS, Kim NU, Park BJ, & Kim JH (2020) In-situ growth of ZIF-8 in amphiphilic graft copolymer for mixed matrix membranes with simultaneous improvement of permeability and selectivity. *Separation and Purification Technology* 253:117514.
30. Jia M, Zhang X-F, Feng Y, Zhou Y, & Yao J (2020) In-situ growing ZIF-8 on cellulose nanofibers to form gas separation membrane for CO2 separation. *Journal of Membrane Science* 595:117579.
31. Jiao C, Li Z, Li X, Wu M, & Jiang H (2021) Improved CO_2/N_2 separation performance of Pebax composite membrane containing polyethyleneimine functionalized ZIF-8. *Separation and Purification Technology* 259:118190.
32. Liu N, Cheng J, Hou W, Yang X, & Zhou J (2021) Pebax‐based mixed matrix membranes loaded with graphene oxide/core shell ZIF-8@ZIF-67 nanocomposites improved CO_2 permeability and selectivity. *Journal of Applied Polymer Science* 138(23):50553.
33. Li X*, et al.* (2020) Enhanced gas separation performance of Pebax mixed matrix membranes by incorporating ZIF-8 in situ inserted by multiwalled carbon nanotubes. *Separation and Purification Technology* 248:117080.
34. Ding R*, et al.* (2020) Amino-functional ZIF-8 nanocrystals by microemulsion based mixed linker strategy and the enhanced CO2/N2 separation. *Separation and Purification Technology* 236.
35. Yang K*, et al.* (2020) Stretched ZIF-8@GO flake-like fillers via pre-Zn(II)-doping strategy to enhance CO2 permeation in mixed matrix membranes. *Journal of Membrane Science* 601.
36. Atash Jameh A, Mohammadi T, & Bakhtiari O (2020) Preparation of PEBAX-1074/modified ZIF-8 nanoparticles mixed matrix membranes for CO2 removal from natural gas. *Separation and Purification Technology* 231:115900.
37. Jain A*, et al.* (2021) 6FDA-DAM:DABA Co-Polyimide Mixed Matrix Membranes with GO and ZIF-8 mixtures for effective CO_2/CH_4 separation. *Nanomaterials* 11(3).
38. Fan Y*, et al.* (2020) Zn(II)-modified imidazole containing polyimide/ZIF-8 mixed matrix membranes for gas separations. *Journal of Membrane Science* 597:117775.
39. Sun J*, et al.* (2019) MOF-801 incorporated PEBA mixed-matrix composite membranes for CO2 capture. *Separation and Purification Technology* 217:229-239.

40. Sánchez-Laínez J*, et al.* (2019) Polymer engineering by blending PIM-1 and 6FDA-DAM for ZIF-8 containing mixed matrix membranes applied to CO_2 separations. *Separation and Purification Technology* 224:456-462.
41. Zhou Y, Jia M, Zhang X, & Yao J (2020) Etched ZIF-8 as a Filler in Mixed-Matrix Membranes for Enhanced CO2 /N2 Separation. *Chemistry* 26(35):7918-7922.
42. Liu B, Li D, Yao J, & Sun H (2020) Improved CO2 separation performance and interfacial affinity of mixed matrix membrane by incorporating UiO-66-PEI@[bmim][Tf2N] particles. *Separation and Purification Technology* 239.
43. Lai W-H, Zhuang G-L, Tseng H-H, & Wey M-Y (2019) Creation of tiny defects in ZIF-8 by thermal annealing to improve the CO2/N2 separation of mixed matrix membranes. *Journal of Membrane Science* 572:410-418.
44. Kang DA, Kim K, Lim JY, Park JT, & Kim JH (2020) Mixed matrix membranes consisting of ZIF-8 in rubbery amphiphilic copolymer: Simultaneous improvement in permeability and selectivity. *Chemical Engineering Research and Design* 153:175-186.
45. Xiao Y, Dai Y, Chung T-S, & Guiver MD (2005) Effects of Brominating Matrimid Polyimide on the Physical and Gas Transport Properties of Derived Carbon Membranes. *Macromolecules* 38(24):10042-10049.
46. Berean K*, et al.* (2014) The effect of crosslinking temperature on the permeability of PDMS membranes: Evidence of extraordinary CO_2 and CH_4 gas permeation. *Separation and Purification Technology* 122:96-104.
47. Chen W-J & Martin CR (1994) Gas-transport properties of sulfonated polystyrenes. *Journal of Membrane Science* 95(1):51-61.
48. Perego G, Roggero A, Sisto R, & Valentini C (1991) Membranes for gas separation based on silylated polyphenylene oxide. *Journal of Membrane Science* 55(3):325-331.
49. Li X-G, Kresse I, Xu Z-K, & Springer J (2001) Effect of temperature and pressure on gas transport in ethyl cellulose membrane. *Polymer* 42(16):6801-6810.